NANOINDENTATION AND FRACTURE ANALYSIS OF THIN SOLID FILMS

K.Sriram, R.Narasimhan and S.K.Biswas

Department of Mechanical Engineering,
Indian Institute of Science,
Bangalore 560012, India

ABSTRACT

In this paper, finite element simulations of spherical nanoindentation of a thin hard film deposited on a soft substrate are carried out. The energy release rate J associated with circumferential cracks extending inwards from the film surface is computed. The mechanics of fracture of the film during nanoindentation is studied by examining the variation of J with crack length and also the stress distributions in the uncracked film. Finally, methods for combining experimental load versus indentation depth data with simulation results in order to obtain the fracture energy of the film are proposed.

1. INTRODUCTION

In recent years, material components with protective surface coatings of micrometric thickness are being used quite extensively in various technological applications. The mechanical performance of these components is critically dependent on the strength and toughness of these films as well as on those of the film-substrate interface. Submicrometer indentation is a popular technique for investigating the mechanical properties such as hardness and elastic modulus of a coated specimen [1]. However, techniques for determining the fracture toughness of the film from nanoindentation test results are not well developed. Experimental studies [2-4] have shown that radial and circumferential cracks (through the film), as well as interfacial failure, may occur during nanoindentation tests. In situations where cracks form through the film, some steps in the load versus displacement response are observed [3,4]. The interpretation of such experimental data to obtain the fracture toughness of the film is generally based on approximate relationships [2], and also requires *a posteriori* measurement of crack lengths from the coated sample which is not a trivial task.

The first step towards providing a sound fracture mechanics methodology for analysing nanoindentation test results was taken by Weppelmann and Swain [4]. They conducted a detailed study of the stress fields that develop during spherical nanoindentation of thin hard films deposited on soft substrates. The focus of this study was to investigate the effects of indenter radius to film thickness ratio and plastic yielding in the substrate on the above fields. The weight function method was employed to compute the stress intensity factors associated with circumferential or cylindrical cracks in the film. However, a systematic investigation of the mechanics of fracture in the film during nanoindentation was not performed in their work. Further, the use of the weight function method entails the assumptions of plane strain (whereas, in reality, the domain is axisymmetric), and small geometry changes in the indented zone.
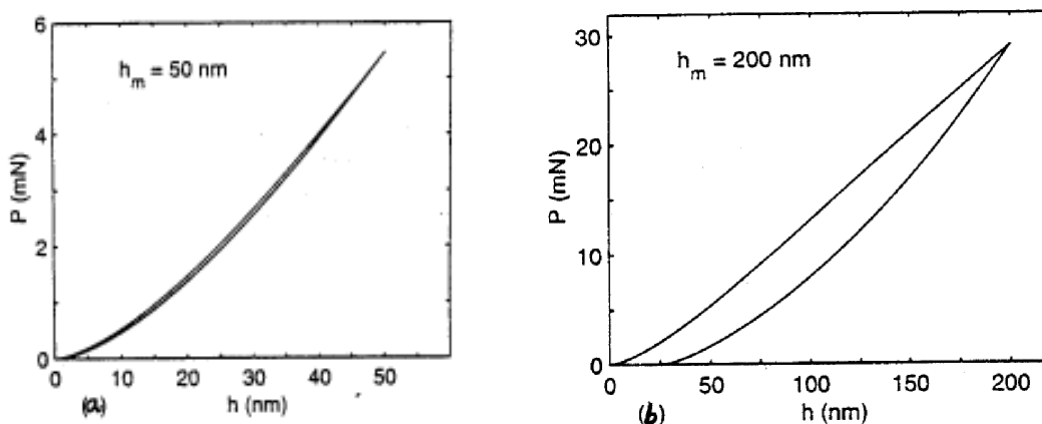
Hence, the primary objective of this paper is to investigate the mechanics of fracture in thin hard films due to occurrence of cylindrical cracks during spherical nanoindentation. The stress fields in the film, as well as the energy release rate associated with cylindrical cracks at different indentation depths are studied using finite element analyses. The film is assumed to be elastic, whereas plastic yielding in the substrate is considered. The energy release rate is computed directly from finite element analyses of cracked samples using the numerically accurate domain integral formulation [5]. Also, methods are proposed by which finite element simulations can be employed to interpret nanoindentation test results and yield information related to fracture behaviour of the film.

2. MODELLING ASPECTS

In this work, axisymmetric finite element analyses of spherical nanoindentation of the film-substrate system is carried out. An updated Lagrangian finite element formulation is employed. The contact between the (rigid) indenter and the film is assumed as frictionless and is modelled using a penalty approach [6]. The radius R_i of the indenter and the thickness t of the film are chosen as 0.67 μm and 1 μm, respectively. The radial dimension R_s of the film-substrate system and the substrate thickness t_s are taken as 0.2 mm and 0.1 mm respectively, so that boundary effects do not influence the stress distribution near the zone of indentation. The film is assumed to be linear elastic with Young's modulus E and Poisson's ratio ν taken as 480 GPa and 0.2, respectively, which correspond to TiN. A finite deformation, J_2 flow theory of plasticity model is employed for the substrate, with E, ν, initial yield strength σ_{ys} and tangent modulus E_t chosen as 210 GPa, 0.3, 600 MPa and 7.25 GPa, respectively, which pertain to an intermediate strength steel.

3. STRESS ANALYSIS

It is important to understand the stress variations in the film during indentation before investigating the mechanics of indentation fracture. To this end, indentation analysis of an uncracked film-substrate system is undertaken in this section. The variations of load P versus indentation depth h are shown in Figs.1(a) and (b). These figures pertain to maximum indentation depth h_m = 50 and 200 nm, respectively. The corresponding contact radii a are 170 and 295 nm, respectively. Both the loading and unloading segments (starting from the maximum indentation depth) are displayed in Figs.1(a) and (b).
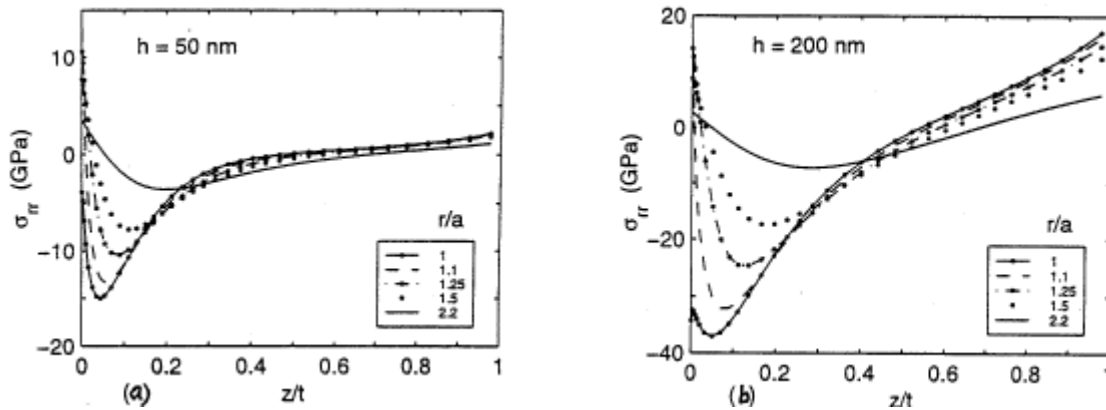

Figure 1: Load versus indentation depth for the uncracked film corresponding to maximum indentation depth of **(a)** h_m = 50 nm and **(b)** h_m = 200 nm.

It is observed from Fig.1a that the unloading curve almost coincides with the loading curve at low indentation depth, whereas it deviates substantially from the loading curve at large indentation depth (see Fig.1b). This is attributed to a significantly large plastic zone size in the substrate at large indentation depth. Thus, it was found from contours of plastic strain that the maximum plastic zone size in the substrate at $h = 50$ and 200 nm are 760 and 3100 nm, respectively.

The radial stress σ_{rr} at the film surface ($z = 0$) is compressive within the contact zone ($r < a$) [4]. However, the magnitude of σ_{rr} decreases as r increases within the contact zone and it becomes tensile as $r \rightarrow a$. It attains a peak tensile value just outside the contact zone (at r/a between 1 to 1.1). This implies that fracture in the form of cylindrical cracks just around the contact zone may occur during indentation [4]. Hence, in the fracture analyses conducted later, cylindrical cracks located just outside the contact zone, at different indentation depths are studied.
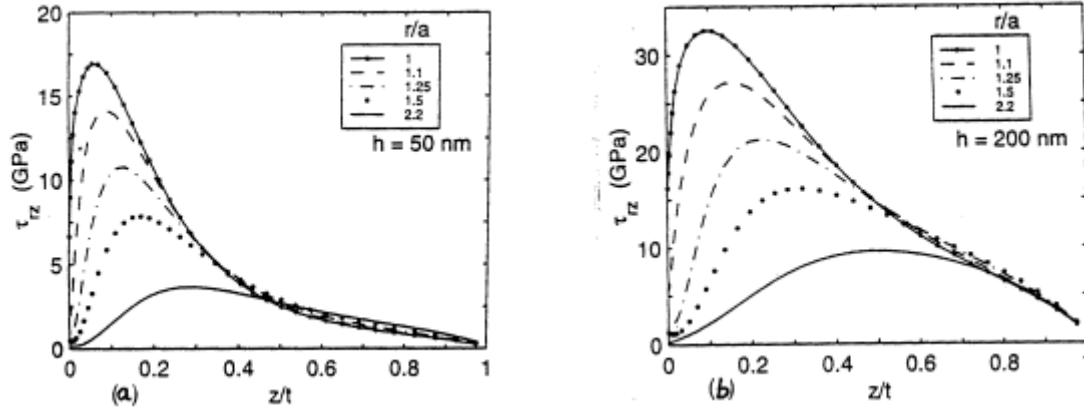
The variations of σ_{rr} with normalized distance z/t through the film thickness corresponding to $h = 50$ and 200 nm are shown in Figs.2(a) and (b), respectively. In these figures, the through thickness variations of σ_{rr} at different radial distances r/a are presented.

Figure 2: Variations of radial stress with normalized distance z/t through the film thickness at different radial locations r/a : **(a)** $h = 50$ nm and **(b)** $h = 200$ nm.

In all cases, σ_{rr} decreases rapidly from the tensile value at the surface and becomes compressive at a small distance z below the surface. It reaches a peak compressive value between $z = 0.1t$ to $0.2t$, and thereafter, increases. It may be seen from Fig.2(a) that at low indentation depths σ_{rr} has a very small magnitude for $z > 0.4t$. On the other hand, at large indentation depth, σ_{rr} becomes strongly tensile for $z > 0.4t$ (see Fig.2(b)). Thus, for $h = 200$ nm, $\sigma_{rr} = 17$GPa at r/a close to 1 and $z/t = 1$ (i.e., at the film-substrate interface).

The variations of shear stress τ_{rz} with normalized distance z/t through the film thickness at different radial locations r/a corresponding to $h = 50$ and 200 nm are shown in Figs.3(a) and (b), respectively.
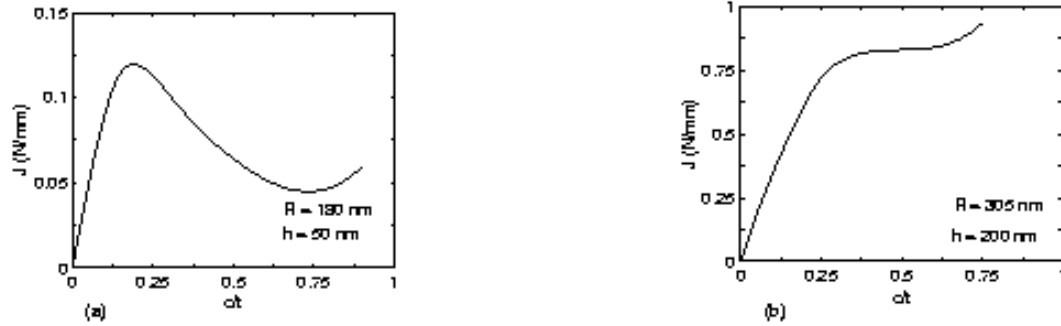
Figure 3: Variations of shear stress with normalized distance z/t through the film thickness at different radial locations r/a : **(a)** h = 50 nm and **(b)** h = 200 nm.

It may be observed from these figures that for all radial distances r/a > 1, τ_{rz} increases as z increases, reaches a peak value between 0.05t and 0.4t depending upon the radial location, and then decreases. As z/t →1, τ_{rz} is close to zero at all values of r/a. This implies that failure of the film-substrate interface cannot take place under shear. Finally, it may be seen from Figs.3(a) and (b) that at small distances z/t below the film surface, the maximum magnitude of τ_{rz} occurs at r/a close to 1 and decreases rapidly as r/a increases. By contrast, all curves shown in Figs.3(a) and (b) almost merge with each other in the range z/t > 0.4.

4. FRACTURE ANALYSIS

In this section, cylindrical cracks extending inwards from the film surface are introduced at different radial distances R. The indentation analysis is conducted till the contact zone approaches the crack surface. The normalized crack length, c/t , is varied from 0.1 to 0.9. The dimensions of the film-substrate system, radius of the indenter, other modelling aspects, and material properties are the same as mentioned in Section 2. The compressive radial stress prevailing below the film surface (see Fig. 2) leads to crack closure for shallow cracks and at small indentation depths. In these cases, the contact between the crack faces is also assumed to be frictionless and the associated constraints are imposed by the penalty approach [6]. On the other hand, there is opening of the crack faces due to tensile radial stress for deep cracks at large indentation depths and, hence, a mixed mode state prevails near the tip under these conditions. The energy release rate J is computed from the finite element results continuously throughout the indentation analysis using the domain integral method [5]. To this end, several rectangular domains of dimensions varying from 10 nm × 10 nm to 125 nm × 125 nm about the crack tip are considered. It is found that J computed from various domains differ by less than three percent.

The variation of J with normalized crack length c/t for cracks located at radial distances R = 180 and 200 nm, respectively, are shown in Figs. 4(a) and (b). These figures pertain to indentation depths of h = 50 and 200 nm, respectively.
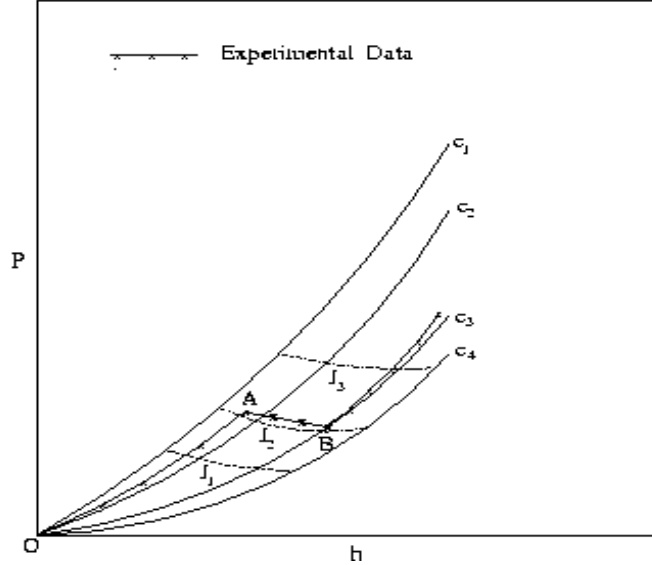
Figure 4: Variation of energy release rate J with normalized crack length c/t for cracks located **(a)** at R=180 nm corresponding to h=50 nm and **(b)** at R=305 nm corresponding to h=200 nm.

On examining Fig.4(a) which pertains to small indentation depth, it may be seen that J increases initially with crack length and reaches a peak at around c = 0.2t. It then decreases between c = 0.2t and 0.75t, and then shows a marginal increase for c > 0.75t. It can be seen from Fig.4(b) that at h = 200 nm, the decreasing branch of the J versus c/t curve has completely vanished, although J remains almost constant over the range of c/t from 0.3 to 0.6. The above trends can be understood by examining the stress distributions shown in Figs. 2 and 3. As already mentioned, shallow cracks are subjected essentially to Mode II loading since σ_{rr} is compressive leading to crack closure. Now, it may be recalled from Fig.3 that τ_{rz} at r/a = 1.1 reaches a peak value at z between 0.1 and 0.2t and, thereafter, decreases with increase in z. This leads to the drastic reduction in J with c/t, for c/t > 0.2 in Fig. 4(a). However, since σ_{rr} is strongly tensile as the film-substrate interface is approached at large indentation depth (see Fig.2(b)), it offsets any reduction in J caused by decrease in τ_{rz} with z/t. Hence, J increases monotonically with c/t in Fig.4(b).

The decreasing branch of the J versus c/t curve (between c/t = 0.2 and 0.75) in Fig.4(a) implies that crack growth over this range of crack lengths will be stable. In other words, the indentation depth will have to increase gradually in order to sustain further crack growth. In the case of Fig.4(b), crack growth will be unstable over the entire range of c/t from 0 to 1 since $\partial J/\partial c > 0$.

5. INTERPRETATION OF EXPERIMENTAL DATA

In Fig.5, a schematic illustration of an experimental P versus h curve with a step AB, which presumably corresponds to the growth of a cylindrical crack located at a radius R from the axis of symmetry, (similar to that observed in [4]), is presented. In order to estimate the fracture energy, J_f, of the film from this experimental curve, the extent of crack growth Δc must be first determined. To this end, a family of P versus h curves corresponding to different crack lengths c_1, c_2, etc., at the observed radial location R, generated by finite element analyses, are superimposed on the experimental data as shown in Fig.5. From this diagram, the extent of crack growth associated with the step AB may be deduced to be around $\Delta c = c_3 - c_2$.

Figure 5: Schematic illustration showing experimental P versus h data superimposed on a nomogram consisting of numerically generated P - h curves corresponding to different crack lengths c_i and constant J trajectories.

The fracture energy J_f of the film may now be estimated in two ways. In the first method, J_f may be calculated as $A_f/(2\pi R\Delta c)$, where A_f is the area of the curved wedge OAB in Fig.5. Alternatively, J_f may be deduced by conducting further analysis of the results and plotting constant J trajectories corresponding to levels J_1, J_2 etc., along with the P versus h curves, as shown by the dash-dot lines in Fig.5. It may be seen from Fig.5 that the step AB in the experimental data lies close to the constant J line pertaining to the level J_2. Hence, J_f may estimated to be equal to J_2.

6. CONCLUSIONS

The radial stress is compressive below the film surface which leads to crack closure for shallow cracks and at low indentation depths. Thus, under these conditions, cylindrical cracks in the film are loaded under mode II and the energy release rate shows a decreasing branch for range of crack lengths between 0.2t and 0.75t. This implies that crack growth will be stable in this range and will occur under gradually increasing h. However, at large h, since σ_{rr} becomes tensile adjacent to the interface, J does not display any decrease with c and crack growth is expected to be completely unstable. Two methods for interpreting experimental P-h data and obtaining the fracture energy J_f of the film have been proposed.

REFERENCES

1. Phar, G.M. and Oliver, W.C. (1992) *MRS Bulletin* 28.
2. Haanappel, V.A.C., Vendel, D.V.D., Metselaar H.S.C., Van Corbach H.D., Fransen T. and Gellings, P.J. (1995) *Thin Solid Films* 254, 153.
3. Whitehead, A.J. and Page, T.F. (1992) *Thin Solid Films* 220, 277.
4. Weppelmann, E. and Swain, M.V. (1996) *Thin Solid Films* 286, 111.
5. Nakamura, T., Shih, C.F. and Freund, L.B. (1986) *Engng. Fract. Mech.* 25, 333.
6. Wriggers, P., Vu Wan, T. and Stein, E. (1990) *Comput. Struct.* 37, 319.